coatings

MDPI

Article

Effect of Al_2O_3 and SiO_2 Inert-Fillers on the Microstructural Evolution and High Temperature Oxidation Resistance of B Modified Silicides Coatings Prepared by Pack Cementation Technology

Linfen Su [1,2,*], Guanqun Zhuo [1,2], Haiwen Song [1,2], Jianyong Yang [1,2] and Kaiyong Jiang [1,2]

[1] College of Mechanical Engineering and Automation, Huaqiao University, Xiamen 361021, China; zhuoguanqun@hqu.edu.cn (G.Z.); songhw@hqu.edu.cn (H.S.); yangjy@hqu.edu.cn (J.Y.); jiangky@hqu.edu.cn (K.J.)
[2] Fujian Key Laboratory of Special Energy Manufacturing, Huaqiao University, Xiamen 361021, China
* Correspondence: linfensu@hqu.edu.cn

Abstract: In this study, B modified silicide coatings were prepared on Nb-Si based alloy with Al_2O_3 or SiO_2 inert-filler by pack cementation technology. Both coatings primarily consisted of a $(Nb,X)Si_2$ with a $(Nb,X)B_2$ + $(Nb,X)Si_2$ outer layer. After oxidation at 1250 °C for 100 h, the coatings showed good oxidation resistance due to the formation of a dense silica. The oxidation products of the coating prepared with Al_2O_3 inert-filler consisted of SiO_2, TiO_2 and Cr_2O_3, while that of the coating prepared with SiO_2 inert-filler consisted of SiO_2, TiO_2, Cr_2O_3, and HfO_2. The different oxidation products may be due to the different oxidation process of these two sample at initial oxidation stage.

Keywords: Nb-Si based alloy; inert-filler; Si-B coating; oxidation resistance

Citation: Su, L.; Zhuo, G.; Song, H.; Yang, J.; Jiang, K. Effect of Al_2O_3 and SiO_2 Inert-Fillers on the Microstructural Evolution and High Temperature Oxidation Resistance of B Modified Silicides Coatings Prepared by Pack Cementation Technology. *Coatings* **2021**, *11*, 700. https://doi.org/10.3390/coatings11060700

Academic Editor: Maria Vittoria Diamanti

Received: 16 April 2021
Accepted: 8 June 2021
Published: 11 June 2021

1. Introduction

The Nb-Si based alloys have attracted significant research interest as the promising candidate for high temperature structure materials due to their excellent mechanical properties at high temperatures [1–3]. However, the widespread use of Nb−Si based alloys is limited as their oxidation resistance is still inadequate, which may be due to the formation of non-protective oxides (Nb_2O_5, $CrNbO_4$, $Ti_2Nb_{10}O_{29}$, and $TiNbO_4$) at high temperatures [4–7]. Alloying with elements such as Ti, Al, Cr, Sn, Ta, and Ge could moderately increase their high temperature oxidation resistance [8–11]. However, further alloying usually leads to deterioration of their mechanical properties [3,12,13]. Consequently, deposition of coatings that can form dense, adherent and slow growing oxide scales is considered an effective way to address the requirement of the enhanced oxidation resistance and high-strength of Nb−Si based alloys [14,15].

Aluminide and silicide coatings, which can produce continuous Al_2O_3 and SiO_2 scales at high temperature, have been widely studied [16–18]. In particular, silicide coatings are more attractive due to their higher application temperature. Among various coating preparation techniques, pack cementation is considered an effective way to prepare silicide coatings, owing to its simple process [19]. The substrates are embedded into a powder mixture consisting of depositing elements as a donor, a halide salt as an activator, and an inert-filler. The effects of donor, activator, and prepared condition on the coating microstructure have been widely investigated. Zhou et al. [20] have used the TiB_2 as the boron source to form a B-modified silicide coating, which exhibited good oxidation resistance at both high and intermediate temperature. Qiao et al. [21] have investigated the effect of the amount of B powder on the microstructural evolution and oxidation resistance of the coating. Cockeram and Rapp [22] have investigated the effect of different activators (NaF, MgF_2, AlF_3 and CuF_2) on the oxidation resistance of $MoSi_2$ coating, revealing that

the NaF-base byproduct layer provided outstanding protection against the catastrophic disintegration of the $MoSi_2$ coatings at low temperature. Although few studies have focused on the effect of the inert-filler on the microstructural evolution and oxidation resistance of the Si−B coating, some investigations are conducted in other refractory alloys. For Ni substrate, the chromizing coating using CeO_2 + Al_2O_3 filler exhibited better oxidation resistance than that prepared with only Al_2O_3 filler, as the addition of CeO_2 in Al_2O_3 can significantly retard the grain growth of the coating [23]. For Mo substrate, the $MoSi_2$ coating prepared with SiO_2 filler showed the best oxidation resistance, while the coating prepared with SiC filler exhibited the thickest $MoSi_2$ layer [24]. In the present work, Si−B coatings were prepared on a Nb-Si based alloy; Si and TiB_2 were selected as the donor, NaF was selected as the activator, and the Al_2O_3 or SiO_2 was selected as the inert-filler. The effects of different inert-fillers on the microstructure evolution and high temperature oxidation resistance were investigated. Furthermore, the coating formation and oxidation mechanism of Si-B coatings were discussed.

2. Materials and Methods

2.1. Materials

Substrates (Nb-15Si-24Ti-13Cr-2Al-2Hf (at.%)) were fabricated by non-consumable arc-melting. The ingots were re-melted and inverted at least four times to guarantee the uniformity of the composition. Samples were cut into Ø10 mm × 3 mm by electro-discharge machining. These samples were polished on wet SiC paper to 800 grit, then ultrasonically washed in an alcohol machine and dried for 1 h.

2.2. Coating Preparation

Powder mixtures with 8 wt.% Si (99.9 wt.% purity), 8 wt.% TiB_2 (99.9 wt.% purity), 5 wt.% NaF (99.9 wt.% purity), and 79 wt.% Al_2O_3 (99.9 wt.% purity) or SiO_2 (99.9 wt.% purity) were chosen as inert-filler respectively. The average diameters of Al_2O_3 and SiO_2 filler were 5.8 um and 12.4 μm, respectively. Each powder was first ground in a ball miller for 1 h to ensure composition homogeneity. Next, the substrate and mixed pack were put into an alumina retort and the substrate was completely covered by the powder. The retort was heated in a tube furnace at a rate of 5 °C/min and kept at 1300 °C for 10 h. The tube furnace was filled with high-purity argon (99.99 wt.% purity) until the tube furnace was cooled to room temperature.

2.3. Oxidation Test

Prior the oxidation test, the alumina crucible was placed at 1250 °C for 2 h to assure the quality of crucible was stable. Then each sample was put in a separate alumina crucible for isothermal oxidation test of 1250 °C. The samples were removed from the furnace at the intervals of 10, 20, 40, 60, 80, and 100 h and the oxidation weight gain of the samples was recorded, using a precision analytical balance (model CPA225D, Sartorius, Göttingen, Germany) with an accuracy of 0.00001 g.

2.4. Characterization

Phase composition of the as-prepared and oxidized coatings was analyzed by X-ray diffraction (XRD SmartLaSmar, Rigaku, Tokyo, Japan) with Cu radiation. The operating parameters were: K-α target with using Cu, scanning speed was 6°/min, the scanning range was 20–90°, and the working voltage and current were 40 kV and 20 mA, respectively. The surface morphologies, i.e., micrographs of cross-sections of the as-prepared and oxidized coatings were observed by scanning electron microscope with an energy dispersive spectroscopy (JSM-IT500, JEOL Ltd., Tokyo, Japan).

3. Results

3.1. Microstructures of B Modified Coatings

Figure 1 shows the XRD patterns of B modified coatings prepared with Al_2O_3 and SiO_2 inert-fillers. Both samples primarily consisted of $(Nb,X)Si_2$ (JCPD 08-0450) and $(Nb,X)B_2$ (JCPD 35-0742) (X represents Ti, Cr, and Hf elements). In addition, it was found that Al_2O_3 and SiO_2 were also detected in the XRD pattern, indicating that inert-fillers were adhered on the coating surface. Figure 2 demonstrates surface morphologies of Si-B coatings. As shown in Figure 2, surface morphologies of both Si-B coatings were relatively dense, with no significant cracks. For the coating prepared with Al_2O_3, a small amount of white, particle-like residual inert-filler Al_2O_3 was adhered to the coating surface. For the coating prepared with SiO_2, some plate-like SiO_2 was covered on the coating surface, suggesting that the residual inert-filler SiO_2 particles melted during the pack cementation process.

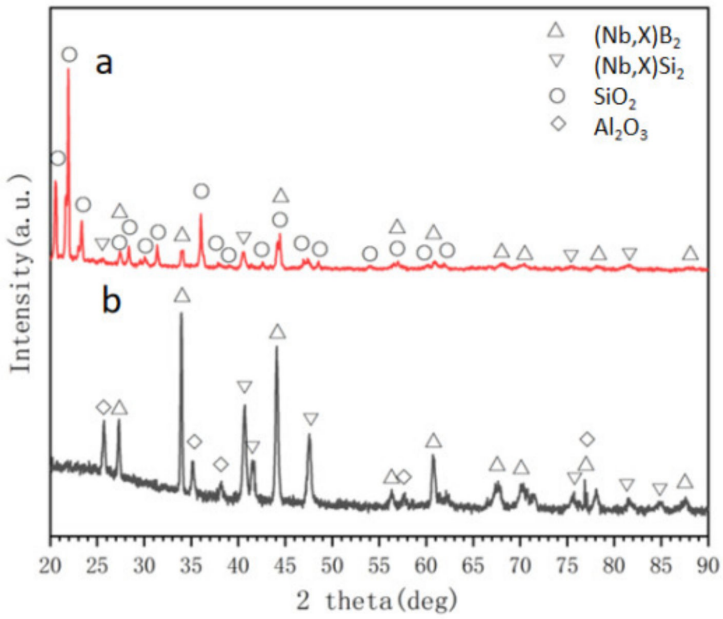

Figure 1. X-ray patterns of B modified silicides coatings prepared with Al_2O_3 (**a**) and SiO_2 (**b**).

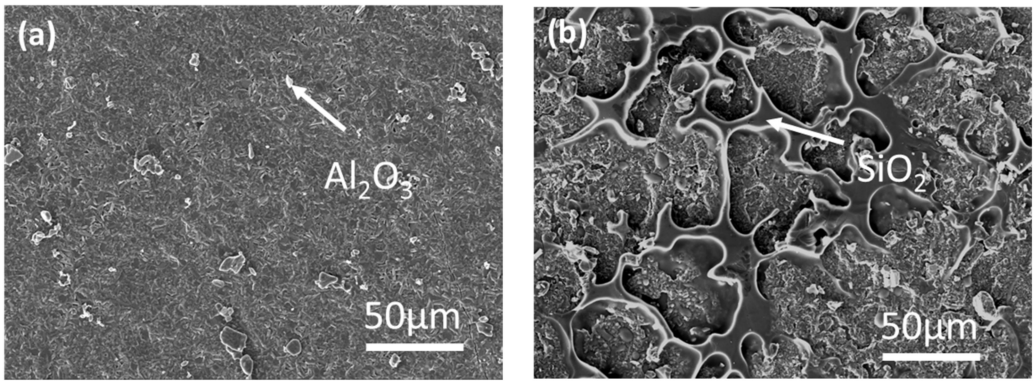

Figure 2. SE image of surface morphologies of B modified silicides coatings prepared with Al_2O_3 (**a**) and SiO_2 (**b**).

Figure 3 shows cross-section microstructures of B modified coatings prepared with Al_2O_3 and SiO_2 inert-fillers. Table 1 presents the element composition of B modified coatings. Both coatings consisted of a $(Nb,X)B_2$ + $(Nb,X)Si_2$ outer layer, a $(Nb,X)Si_2$ intermediate layer, and a $(Nb,X)_5Si_4$ inner layer, as confirmed by XRD (Figure 1) and EDS (Table 1),

which was in agreement with the study of Zhou et al. [20]. In addition, it was found that white particles and blocks (as shown in Figure 3) dispersed in the intermediate and transitional layers have a higher content of Hf, which were confirmed to be Hf-rich $(Nb,X)Si_2$ and Hf-rich $(Nb,X)_5Si_4$, respectively. The thickness of B modified coatings prepared with Al_2O_3 and SiO_2 inert-fillers were 198 ± 3 and 178 ± 2 μm, respectively.

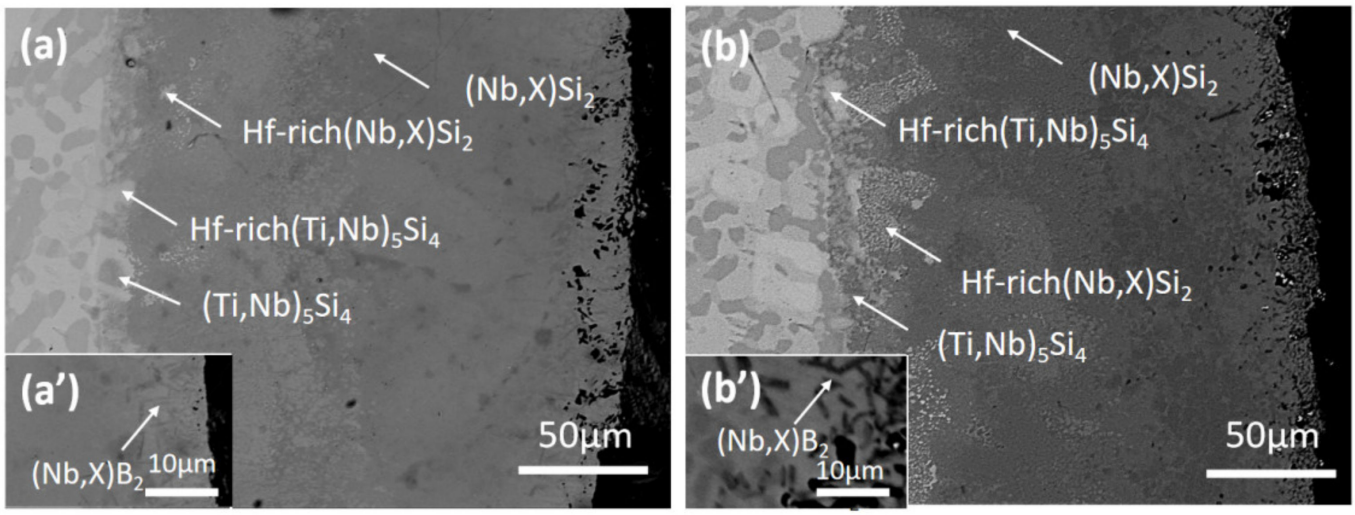

Figure 3. BSE image of cross-section morphologies of B modified silicides coatings prepared with Al_2O_3 (**a**) and SiO_2 (**b**); (**a'**) and (**b'**): enlarge BSE images of the outer layer of the coatings.

Table 1. Element composition (at.%) of B modified silicides coatings prepared with Al_2O_3 and SiO_2 filler.

Sample	Phase	Composition					
		B	Si	Ti	Cr	Nb	Hf
Sample prepared with Al_2O_3	$(Nb,X)B_2$	45.4 ± 0.9	23.4 ± 0.1	17.8 ± 0.4	0.8 ± 0.1	11.6 ± 0.7	0.9 ± 0.2
	$(Nb,X)Si_2$	-	65.2 ± 0.2	9.5 ± 0.7	6.0 ± 0.1	18.2 ± 0.6	1.1 ± 0.1
	Hf-rich $(Nb,X)Si_2$	-	44.0 ± 0.5	25.0 ± 0.9	5.7 ± 0.8	21.3 ± 0.5	4.1 ± 0.3
	$(Nb,Ti)_5Si_4$	-	43.1 ± 0.5	24.6 ± 0.2	4.8 ± 0.6	26.4 ± 0.7	1.2 ± 0.2
	Hf-rich $(Nb,X)_5Si_4$	-	41.7 ± 0.4	25.7 ± 0.9	3.4 ± 0.6	25.2 ± 0.5	4.1 ± 0.5
Sample prepared with SiO_2	$(Nb,X)B_2$	46.2 ± 0.3	21.5 ± 0.1	15.8 ± 0.8	1.8 ± 0.3	13.5 ± 0.1	1.3 ± 0.2
	$(Nb,X)Si_2$	-	59.8 ± 0.9	10.0 ± 0.4	3.5 ± 0.9	25.7 ± 0.4	1.0 ± 0.1
	Hf-rich $(Nb,X)Si_2$	-	50.6 ± 0.8	16.8 ± 0.2	2.9 ± 0.4	24.0 ± 0.5	5.7 ± 0.2
	$(Nb,Ti)_5Si_4$	-	45.1 ± 0.3	18.9 ± 0.1	11.2 ± 0.1	23.4 ± 0.7	1.4 ± 0.3
	Hf-rich $(Nb,X)_5Si_4$	-	42.9 ± 0.1	22.6 ± 0.9	9.0 ± 0.6	21.3 ± 0.1	4.3 ± 0.7

3.2. Oxidation Resistance of B Modified Coatings

Figure 4 demonstrates the oxidation weight gain curves of B modified coatings samples. The weight gains of the samples prepared with Al_2O_3 and SiO_2 after oxidation at 1250 °C for 100 h were 2.77 mg cm^{-2} and 2.31 mg cm^{-2}, respectively. In our previous study [18], the Nb-Si bases alloy without coating experiences linear oxidation with a weight gain of 87.6 mg/cm^2 after oxidation at 1250 °C for 100 h, suggesting that the coatings showed good oxidation resistance protecting the substrate from oxidation. The oxidation mechanism of B modified coating conforms to the parabolic law (Figure 4b) according to Equation (1) [9]:

$$\left(\frac{\Delta m}{A}\right)^2 = kt \quad (1)$$

where Δm, A, and t are the mass variation, the total surface area of sample and the oxidation time, respectively. The value of k determines the oxidation rate of sample. The parabolic

rate constants ($g^2\ cm^{-4}\ s^{-1}$) of the samples prepared with Al_2O_3 and SiO_2 are calculated to be 2.13×10^{-11} and 1.48×10^{-11}, respectively.

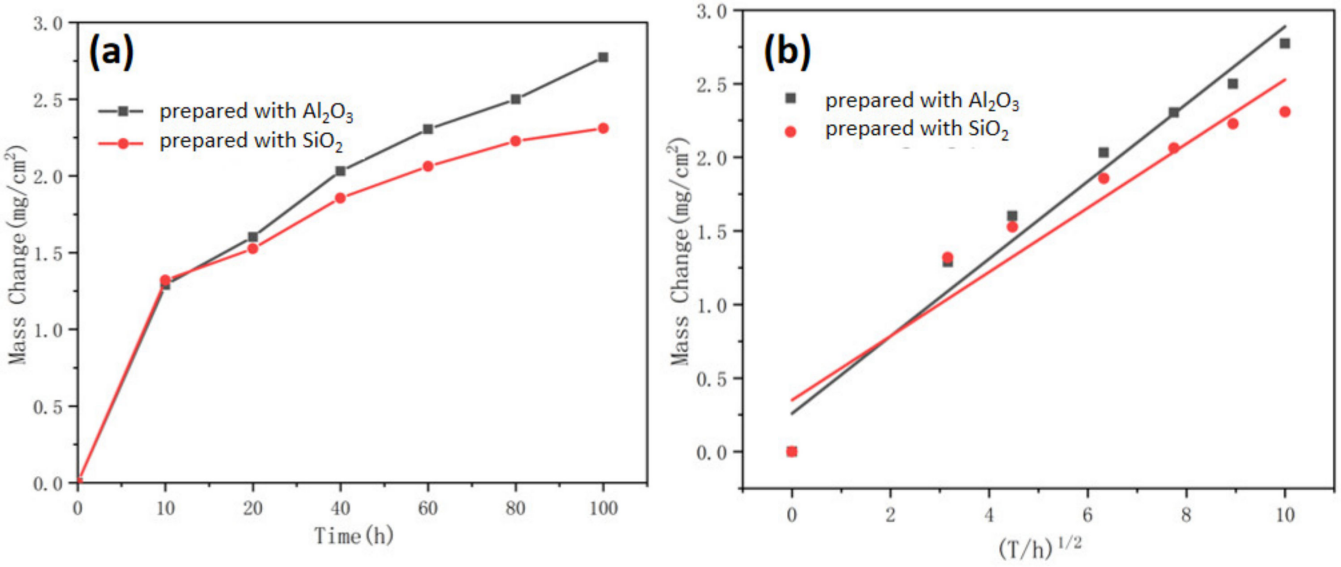

Figure 4. (**a**) Oxidation curve of B modified silicides coatings prepared with Al_2O_3 and SiO_2 inert-filler at 1250 °C for 100 h; (**b**) representation of the weight gain versus the square root of time for the B modified coatings.

3.3. Oxidation Products and Microstructure of Oxide Scale

Figure 5 demonstrates the XRD patterns of B modified coatings after oxidation at 1250 °C for 1, 10, and 100 h. The oxidized coating prepared with Al_2O_3 inert-filler mainly consisted of TiO_2 (JCPD 21-1276), SiO_2 (JCPD 39-1425) and Cr_2O_3 (JCPD 38-1479), while the oxidized coating prepared with SiO2 inert-filler mainly consisted of TiO_2, SiO_2, Cr_2O_3, and HfO_2 (JCPD 40-1173). Figure 6 shows surface morphologies of oxidized B modified coatings after oxidation at 1250 °C for 1, 10, and 100 h. For the coating prepared with Al_2O_3 inert-filler, the surface scale mainly consisted of a dark, dense glass-like phase, distributed with a rod-like phase. EDS analysis demonstrated that the glass-like phase had a composition of 61.4O-33.3Si-1.4Ti-0.4Cr-1.3Nb (at.%), which indicated that it was SiO_2, while the rod-like phase had a composition of 54.4O-38.5Ti-2.94Cr at.%), which indicated that it was TiO_2. For the coating prepared with SiO_2 inert-filler, the surface scale mainly consisted with a dark, dense glass-like phase, distributed with a rod-like phase and a particle-like phase. According to EDS analysis the glass-like phase and the rod-like phase were also the SiO_2 and TiO_2, respectively. The particle-like phase had a composition of 74.9O-1.8Ti-23.3Hf (at.%), which indicates that it is HfO_2. It could be concluded that the HfO_2 phase appeared in the sample prepared with SiO_2 inert-filler.

Figure 7 demonstrates the cross-section microstructures of oxidized B modified coatings after oxidation at 1250 °C for 1, 10, and 100 h. Table 2 presents the element composition of oxidized B modified coatings. As shown in Figure 7, the uniform and continuous SiO_2 oxide scales were formed and adhered tightly on the coatings. For the coating prepared with Al_2O_3 inert-filler, the dark matrix and rod-like phase were confirmed to be SiO_2 and TiO_2, respectively, according to EDS analysis. For the oxide scales formed after oxidation for 1 and 10 h, the upper layer of the oxide scale consisted of SiO_2 and TiO_2, while the lower layer of the oxide scale consisted of SiO_2, TiO_2, and Cr_2O_3 according to the BSE and EDS results (Figures 5 and 7, Table 2). To further increase the oxidation time to 100 h, the lower layer of the oxide scale was changed to a continuous Cr_2O_3 layer (as shown in Figure 7c).

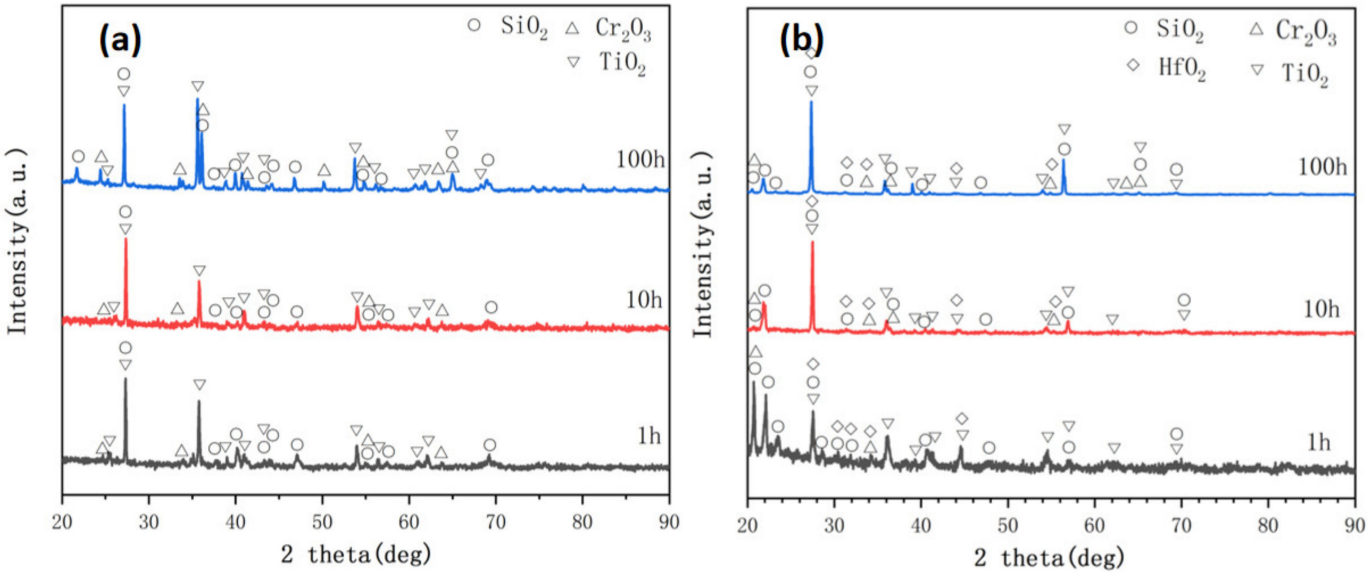

Figure 5. X-ray patterns of B modified silicides coatings prepared with Al_2O_3 (**a**) and SiO_2 (**b**) after oxidation at 1250 °C.

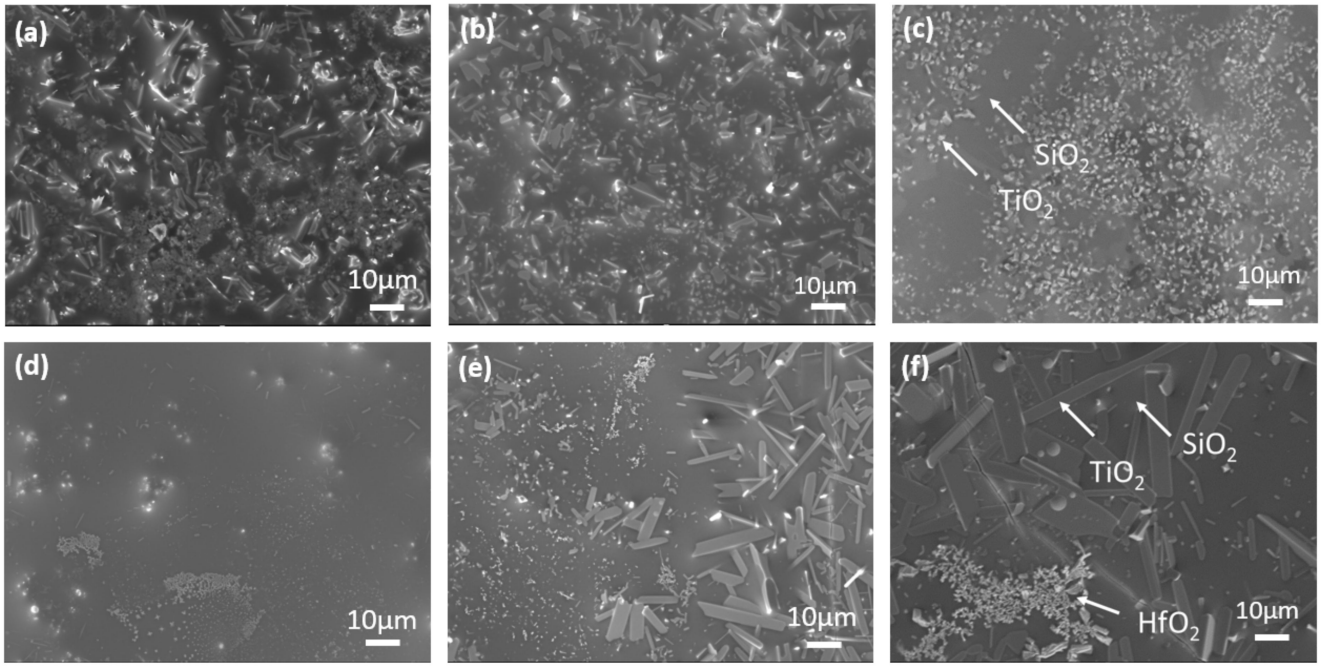

Figure 6. SE image of surface morphologies of oxidized B modified silicides coatings prepared with Al_2O_3 (**a**–**c**) and SiO_2 (**d**–**f**) after oxidation at 1250 °C for 1 h (**a**,**d**), 10 h (**b**,**e**), and 100 h (**c**,**f**).

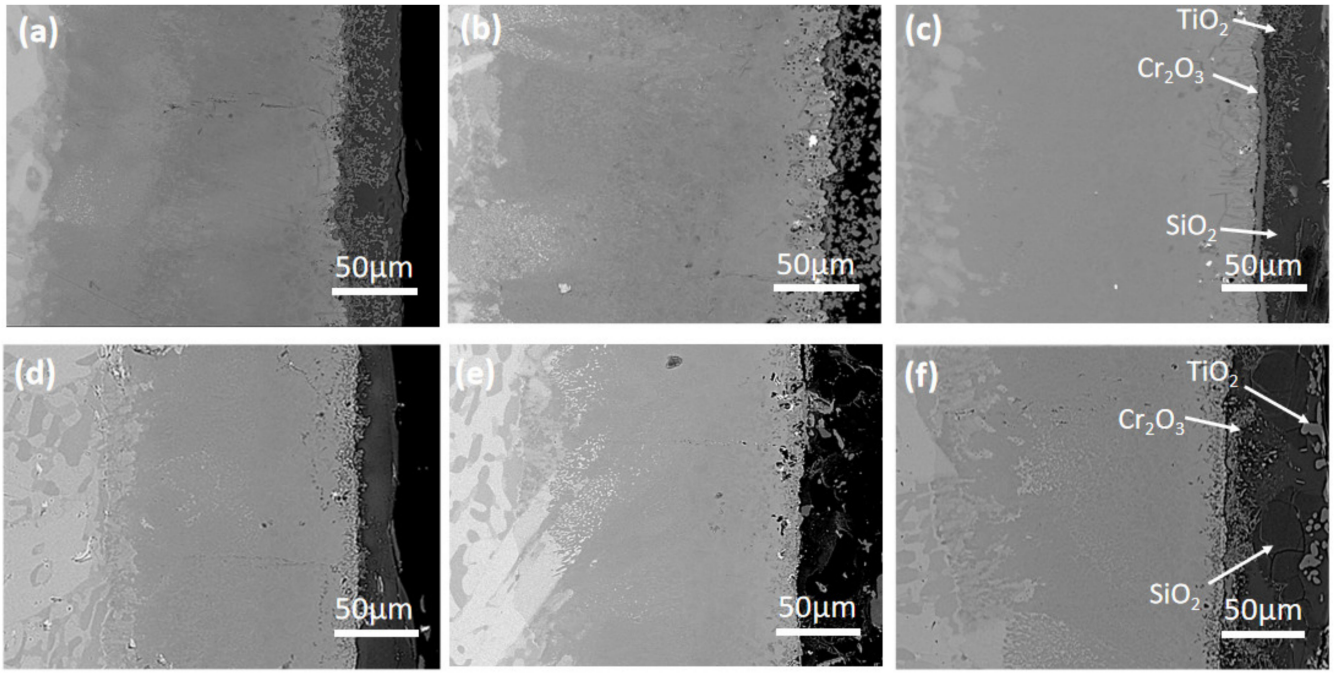

Figure 7. BSE image of cross-section morphologies of oxidized B modified silicides coatings prepared with Al_2O_3 (**a**–**c**) and SiO_2 (**d**–**f**) after oxidation at 1250 °C for 1 h (**a**,**d**), 10 h (**b**,**e**), and 100 h (**c**,**f**).

Table 2. Element composition (at.%) of B modified silicides coatings prepared with Al_2O_3 and SiO_2 filler after oxidation at 1250 °C for 100 h.

Sample	Phase	Composition						
		B	**Si**	**Ti**	**Cr**	**Nb**	**Hf**	**O**
Sample prepared with Al_2O_3	$(Nb,X)B_2$	53.6 ± 0.9	17.6 ± 0.6	17.7 ± 0.2	1.4 ± 0.2	7.7 ± 0.4	2.0 ± 0.9	-
	$(Nb,X)Si_2$	-	63.5 ± 0.5	10.7 ± 0.5	2.4 ± 0.6	22.7 ± 0.7	0.7 ± 0.1	-
	Hf-rich $(Nb,X)Si_2$	-	57.7 ± 0.4	11.7 ± 0.1	1.5 ± 0.2	25.9 ± 0.4	3.1 ± 0.6	-
	$(Nb,Ti)_5Si_4$	-	43.0 ± 0.4	17.6 ± 0.5	9.1 ± 0.1	28.9 ± 0.8	1.5 ± 0.1	-
	Hf-rich $(Nb,X)_5Si_4$	-	41.0 ± 0.7	26.0 ± 0.3	3.5 ± 0.2	25.4 ± 0.2	4.1 ± 0.1	-
	SiO_2	-	32.4 ± 0.9	1.4 ± 0.1	0	0	2.1 ± 0.1	62.3 ± 0.8
	TiO_2	-	0	26.1 ± 0.2	6.8 ± 0.1	0	0	57.2 ± 0.4
	Cr_2O_3	-	0	0.4 ± 0.1	46.5 ± 0.9	0	0	52.9 ± 0.9
Sample prepared with SiO_2	$(Nb,X)B_2$	46.9 ± 0.9	17.6 ± 0.7	22.4 ± 0.7	0.8 ± 0.1	10.9 ± 0.1	1.3 ± 0.1	-
	$(Nb,X)Si_2$	-	60.8 ± 0.5	8.3 ± 0.1	3.9 ± 0.2	26.2 ± 0.1	0.9 ± 0.3	-
	Hf-rich $(Nb,X)Si_2$	-	51.5 ± 0.1	16.3 ± 0.5	1.9 ± 0.2	27.0 ± 0.2	3.3 ± 0.1	-
	$(Nb,Ti)_5Si_4$	-	42.7 ± 0.4	19.9 ± 0.7	8.2 ± 0.8	27.6 ± 0.8	1.7 ± 0.1	-
	Hf-rich $(Nb,X)_5Si_4$	-	41.7 ± 0.5	13.6 ± 0.2	1.4 ± 0.5	41.0 ± 0.1	2.4 ± 0.1	-
	SiO_2	-	32.3 ± 0.3	1.6 ± 0.6	0	0	0.3 ± 0.1	65.1 ± 0.7
	TiO_2	-	0	35.8 ± 0.8	0	0	0	64.3 ± 0.9
	Cr_2O_3	-	0	0.8 ± 0.1	43.4 ± 0.8	0	0	55.6 ± 0.1
	HfO_2	-	26.5 ± 0.5	1.1 ± 0.2	0	1.7 ± 0.1	10.3 ± 0.3	60.1 ± 0.8

For the coating prepared with SiO_2 inert-filler, a thick SiO_2 was formed after oxidation for 1 h, and the TiO_2 and Cr_2O_3 were mainly distributed at the interface of silica and coating (Figure 7d). Unlike the glass scale of the coating prepared with Al_2O_3 inert-filler, with the oxidation time increasing to 100 h, the lower layer of the oxide scale did not change to a continuous Cr_2O_3, but consisted of SiO_2 and Cr_2O_3 (Figure 7f). HfO_2 was not observed in the cross-sectional microstructures of the scale, suggesting that the HfO_2 was mainly distributed on the surface of the scale.

Remarkably, the thickness of the coating prepared with Al_2O_3 and SiO_2 decreased by 29 ± 1 and 30 ± 2 μm, respectively, compared to that of as-prepared samples after oxidation for 100 h, suggesting that the consumption of both two coating was similar.

4. Discussion

4.1. Formation Mechanism of the Coatings

In this study, B modified coatings were prepared on a Nb-Si based alloy, Si and TiB_2 were selected as the donor material, NaF was selected as the activor, and Al_2O_3 or SiO_2 was selected as the inert-filler. As discussed above, the coatings prepared with Al_2O_3 and SiO_2 inert-filler showed similar coating structures, mainly consisting of $(Nb,X)Si_2$ with a $(Nb,X)B_2$ + $(Nb,X)Si_2$ outer layer. At elevated temperatures, the activator NaF would react with Si and B to form a series of their own halide vapor species, such as SiF_x (x = 1–4), BF_y (y = 1–3) and B_2F_4 [25,26]. The existence of chemical gradient made fluorides diffused to the substrate surface, resulting in the formation of active atoms Si and B [25], which were deposited together on the substrate surface. In addition, the quantity of deposited Si atoms was significantly more than that of the deposited B atoms, as the partial pressure of Si fluoride was higher than that of B fluoride at 1300 °C [20]. Therefore, the B modified coatings mainly consisted of $(Nb,X)Si_2$ with a $(Nb,X)B_2$ + $(Nb,X)Si_2$ outer layer.

The role of inert-filler in the pack was providing the medium surrounding reaction environment. In addition, it was found that the inert filler resided on the coating surface in this study. The theoretical melting point of Al_2O_3 and SiO_2 were 2054 °C and 1723 °C, respectively [23]. However, SiO_2 particles might melt partially on the surface during the pack cementation process, which was in agreement with the study of Sun et al. [23]. Al_2O_3 had much higher melting point than that of SiO_2, thus only a few particles could be found on the coating surface.

4.2. Oxidation Mechanism of the Coatings

As shown in Figure 7, the B modified coatings prepared with Al_2O_3 or SiO_2 inner-filler both showed good oxidation resistance due to the formation of a dense and continuous SiO_2 glass with self-healing ability. Figure 8 shows the oxidation process of the sample prepared with inert-filler Al_2O_3 or SiO_2 are sketched in Figure 8. On the basis of above results, the oxidation products were different in two samples. The oxidized coating prepared with Al_2O_3 inert-filler mainly consisted of TiO_2, SiO_2, and Cr_2O_3, while the oxidized coating prepared with SiO_2 inert-filler mainly consisted of TiO_2, SiO_2, Cr_2O_3, and HfO_2. The integrity of the oxide scale depends on the Pilling Bedworth Ratio (PBR) of oxide, i.e., the ratio of oxide volume produced to metal volume consumed [27]. The PBR values of Nb_2O_5, SiO_2, Cr_2O_3, TiO_2, and HfO_2 were reported to be 2.74, 1.72, 2.02, 1.73, and 1.17, respectively [28]. Typically, a PBR value ranging from 1 to 2 can protect the metal from oxidation, while an excessive PBR value would result in the fracture of the oxide scale [29]. As the oxidation products of the sample prepared with Al_2O_3 or SiO_2 were TiO_2, SiO_2, Cr_2O_3, and HfO_2, their PBR values ranging from 1 to 2, it could produce the dense oxide scale with good oxidation resistance.

According to the ΔG_0-T plots of various oxides [20,30], the ascending order of ΔG_0 at all temperatures were:

$$\Delta G_0\ HfO_2 < \Delta G_0\ TiO_2 < \Delta G_0\ SiO_2 < \Delta G_0\ B_2O_3 < \Delta G_0\ Cr_2O_3 < \Delta G_0\ Nb_2O_5 \quad (2)$$

Therefore, the descending order of stability was $HfO_2 > TiO_2 > SiO_2 > B_2O_3 > Cr_2O_3 > Nb_2O_5$. For the sample prepared with Al_2O_3, the residual inert-filler Al_2O_3 remain particle-like after pack cementation at 1300 °C. As suggested by Qiao et al. [21], the inert-filler Al_2O_3 could enhance the oxidation resistance to some extent. However, Al_2O_3 particles did not melt to cover the coating and protect it from oxidation. Therefore, at the initial oxidation, the coating was exposed to the oxidation environment. Titanium would oxidize primarily to form TiO_2 rods. As the oxidation processed, silicon would oxidize to form SiO_2. Additionally, B_2O_3 can be formed by the outward diffusion of B. The dissolving of

B_2O_3 in the SiO_2 could reduce the viscosity of the glass scale, and increase the coefficients of thermal expansion (CTE) [31]. Thus, the oxide scale has better self-healing ability and a much better match in CTE with the B modified coating, minimizing spallation and cracks of the oxide scale [31]. HfO_2 was not formed in this sample, due to the lower content (2.0 at.%, as shown in Table 1). Then, the outward diffused Cr^{3+} reacted with oxygen and Cr_2O_3 was formed distributed in the interface of the oxide scale and coating. After a certain time of exposure, the upper layer of the oxide scale consisted of aSiO_2 + TiO_2, while the lower layer of the oxide scale consisted of SiO_2 + TiO_2 + Cr_2O_3 (1 h and 10 h, Figure 8a). With the exposure time increasing to 100 h, the lower layer transformed to a continuous Cr_2O_3 layer (Figure 8a) owing to the outward diffusion of Ti^{4+} from the oxide/alloy interface to the oxide/air interface [20,21].

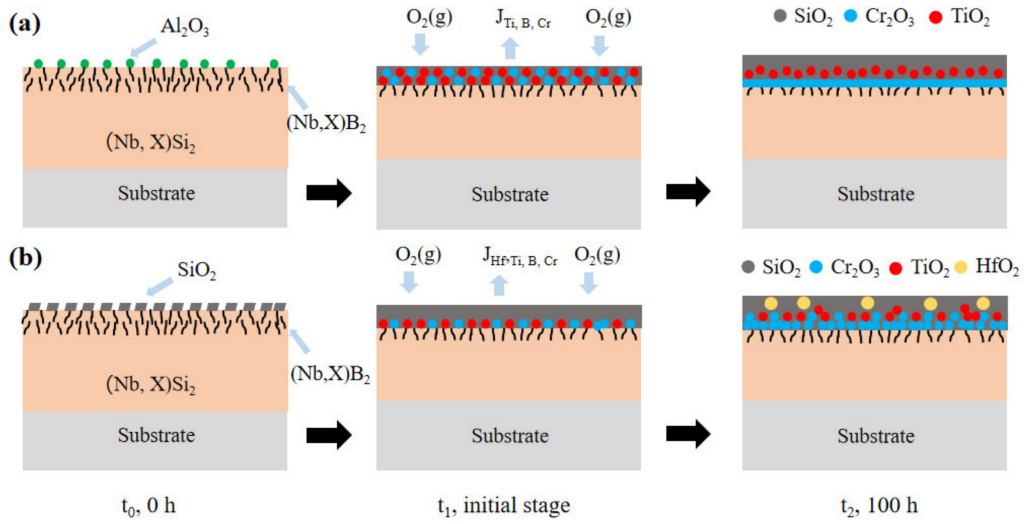

Figure 8. Schematic drawing of oxidation process of B modified silicides coatings at 1250 °C prepared with Al_2O_3 (**a**) and SiO_2 (**b**).

For the sample prepared with SiO_2, the residual inert-filler SiO_2 transformed to plate-like after pack cementation at 1300 °C. During high temperature oxidation, the plate-like residual pack agent SiO_2 would melt into fluid SiO_2 to cover the coating surface, resulting in the rapid formation of a dense SiO_2 layer, thus this sample showed a lower parabolic rate constant as compared to that prepared with Al_2O_3. It was found that the thick SiO_2 layer was formed only after oxidation for 1 h, and the TiO_2 and Cr_2O_3 were mainly distributed at the interface of silica and coating, suggesting that the oxidation process was governed by the inward diffusion of O (Figure 8b). Therefore, HfO_2 was formed due to its lower ΔG value and higher oxygen affinity. The formation mechanism of HfO_2 was similar to the internal oxidation of Nb-Si based alloys, the oxidation process of which was also governed by the inward diffusion of O [9]. HfO_2 has higher melting point (2800 °C) than that of pure SiO_2 [32]. Thus, the dispersion of HfO_2 in SiO_2 glass could increase the melting temperature of the silica. In this sample, TiO_2 and Cr_2O_3 were also formed due to the outward diffusion of Ti^{4+} and Cr^{3+}, as well as the inward diffusion of O. However, the continuous Cr_2O_3 was not formed in this sample, which may be due to the lower parabolic rate constant.

5. Conclusions

1. First item; The B modified coatings prepared with Al_2O_3 and SiO_2 inert-filler mainly consisted of $(Nb,X)Si_2$ with a $(Nb,X)B_2$ + $(Nb,X)Si_2$ outer layer. The Al_2O_3 and SiO_2 inert-fillers were tightly adhered on the coating surface after pack cementation;
2. Second item; After oxidation at 1250 °C for 100 h, the coatings prepared with Al_2O_3 or SiO_2 inert-fillers showed good oxidation resistance due to the formation of a dense

silica. The oxidized coating prepared with Al_2O_3 inert-filler consisted of TiO_2, SiO_2, and Cr_2O_3, while the oxidized coating prepared with SiO_2 inert-filler consisted of TiO_2, SiO_2, Cr_2O_3, and HfO_2;

3. For the coating prepared with SiO_2 inert-fillers, the adherent SiO_2 on the coating would melt partially, resulting in the rapid formation of a dense silica scale during high temperatures. Thus, the oxidation process of this sample was governed by the inward diffusion of O at the initial oxidation stage, leading to a lower parabolic rate constant.

Author Contributions: Conceptualization, L.S. and K.J.; methodology, G.Z. and H.S.; investigation, G.Z. and J.Y.; writing—review and editing, L.S. All authors have read and agreed to the published version of the manuscript.

Funding: This research was funded by National Nature Science Foundation of P.R. China, grant number 51701077, Fujian Nature Science Foundation, grant number 2017J05082 and Promotion Program for Young and Middle-aged Teacher in Science and Technology Research of Huaqiao University, grant number ZQN-PY505.

Institutional Review Board Statement: Not applicable.

Informed Consent Statement: Not applicable.

Data Availability Statement: The raw/processed data required to reproduce these findings cannot be shared at this time as the data also forms part of an ongoing study.

Acknowledgments: The support given are covered by the author contribution and funding sections.

Conflicts of Interest: The authors declare no conflict of interest.

References

1. Perepezko, J.H. The hotter the engine, the better. *Science* **2009**, *326*, 1068–1069. [CrossRef]
2. Bewlay, B.P.; Jackson, M.R.; Subramanian, P.; Zhao, J.-C. A review of very-high-temperature Nb-silicide-based composites. *Met. Mater. Trans. A* **2003**, *34*, 2043–2052. [CrossRef]
3. Zelenitsas, K.; Tsakiropoulos, P. Study of the role of Al and Cr additions in the microstructure of Nb–Ti–Si in situ composites. *Intermetallics* **2005**, *13*, 1079–1095. [CrossRef]
4. Geng, J.; Tsakiropoulos, P.; Shao, G.S. Oxidation of Nb-Si-Cr-Al in situ composites with Mo, Ti and Hf additions. *Mater. Sci. Eng. A* **2006**, *441*, 26–38. [CrossRef]
5. Yao, D.; Cai, R.; Zhou, C.; Sha, J.; Jiang, H. Experimental study and modeling of high temperature oxidation of Nb-base in situ composites. *Corros. Sci.* **2009**, *51*, 364–370. [CrossRef]
6. Voglewede, B.; Rangel, V.R.; Varma, S. The effects of uncommon silicides on the oxidation behavior of alloys from the Nb–Cr–Si system. *Corros. Sci.* **2012**, *61*, 123–133. [CrossRef]
7. Alvarez, D.; Varma, S.K. Characterization of microstructures and oxidation behaviour of Nb-20Si-20Cr-5Al alloy. *Corros. Sci.* **2011**, *53*, 2161–2167. [CrossRef]
8. Su, L.; Jia, L.; Jiang, K.; Zhang, H. The oxidation behavior of high Cr and Al containing Nb-Si-Ti-Hf-Al-Cr alloys at 1200 and 1250 °C. *Int. J. Refract. Met. Hard Mater.* **2017**, *69*, 131–137. [CrossRef]
9. Su, L.F.; Jia, L.N.; Weng, J.F.; Hong, Z.; Zhou, C.G.; Zhang, H. Improvement in the oxidation resistance of Nb-Ti-Si-Cr-Al-Hf alloys containing alloyed Ge and B. *Corros. Sci.* **2014**, *88*, 460–465. [CrossRef]
10. Esparza, N.; Rangel, V.; Gutierrez, A.; Arellano, B.; Varma, S.K. A comparison of the effect of Cr and Al additions on the oxidation behaviour of alloys from the Nb–Cr–Si system. *Mater. High Temp.* **2016**, *33*, 105–114. [CrossRef]
11. Zhang, S.; Jia, L.; Guo, Y.; Kong, B.; Zhou, C.; Zhang, H. Improvement in the oxidation resistance of Nb-Si-Ti based alloys containing zirconium. *Corros. Sci.* **2020**, *163*, 108294. [CrossRef]
12. Ma, R.; Guo, X. Effects of V addition on the microstructure and properties of multi-elemental Nb–Si based ultrahigh temperature alloys. *J. Alloys Compd.* **2020**, *845*, 156254. [CrossRef]
13. Bewlay, B.P.; Jackson, M.R.; Lipsitt, H.A. The balance of mechanical and environmental properties of a multi-element niobium-niobium silicide-based in-situ composite. *Metall. Mater. Trans. A* **1996**, *27*, 3801–3808. [CrossRef]
14. Hou, Q.; Shao, W.; Li, M.; Zhou, C. Interdiffusion behavior of Mo-Si-B/Al2O3 composite coating on Nb-Si based alloy. *Surf. Coat. Technol.* **2020**, *401*, 126243. [CrossRef]
15. Sun, Z.; Tian, X.; Guo, X.; Yin, M.; Zhang, F.; Zhang, X. Oxidation resistance and mechanical characterization of silicide coatings on the Nb-18Ti-14Si-9Al alloy. *Int. J. Refract. Met. Hard Mater.* **2017**, *69*, 18–26. [CrossRef]
16. Hayashi, S.; Takagi, S.; Yamagata, R.; Narita, T.; Ukai, S. Formation of exclusive Al2O3 scale on Nb and Nb-Rich alloys by two-step oxygen–aluminum diffusion process. *Oxid. Met.* **2012**, *78*, 167–178. [CrossRef]

17. Knittel, S.; Mathieu, S.; Portebois, L.; Drawin, S.; Vilasi, M. Development of silicide coatings to ensure the protection of Nb and silicide composites against high temperature oxidation. *Surf. Coat. Technol.* **2013**, *235*, 401–406. [CrossRef]
18. Zhuo, G.; Su, L.; Jiang, K.; Yang, J. Effect of spraying power on oxidation resistance of $MoSi_2$-ZrB_2 coating for Nb-Si based alloy prepared by atmospheric plasma. *Materials* **2020**, *13*, 5060. [CrossRef]
19. Xiang, Z.D.; Rose, S.R.; Burnell-Gray, J.S.; Datta, P.K. Co-deposition of aluminide and silicide coatings on γ-TiAl by pack cementation process. *J. Mater. Sci.* **2003**, *38*, 19–28. [CrossRef]
20. Shao, W.; Wang, W.; Zhou, C. Deposition of a B-modified silicide coating for Nb-Si based alloy oxidation protection. *Corros. Sci.* **2016**, *111*, 786–792. [CrossRef]
21. Qiao, Y.; Shen, Z.; Guo, X. Co-deposition of Si and B to form oxidation-resistant coatings on an Nb–Ti–Si based ultrahigh temperature alloy by pack cementation technique. *Corros. Sci.* **2015**, *93*, 126–137. [CrossRef]
22. Cockeram, B.; Rapp, R.A. The Formation and oxidation resistance of boron-modified and germanium-doped silicide diffusion coatings for titanium and molybdenum. *Mater. Sci. Forum* **1997**, *251–254*, 723–736. [CrossRef]
23. Sun, J.; Fu, Q.-G.; Guo, L.-P.; Liu, Y.; Huo, C.-X.; Li, H.-J. Effect of filler on the oxidation protective ability of MoSi2 coating for Mo substrate by halide activated pack cementation. *Mater. Des.* **2016**, *92*, 602–609. [CrossRef]
24. Meng, J.-S.; Ji, Z.-S. Effect of different fillers on oxidation behavior of low-temperature chromizing coating. *Trans. Nonferrous Met. Soc. China* **2014**, *24*, 1785–1790. [CrossRef]
25. Cockeram, B.; Rapp, R.A. Development and growth of boron-modified and germanium-doped titanium-silicide diffusion coatings by the halide-activated, pack-cementation method. *Oxid. Met.* **1996**, *45*, 375–425. [CrossRef]
26. Mevrel, R.; Duret, C.; Pichoir, R. Pack cementation processes. *Mater. Sci. Technol.* **1986**, *2*, 201–206. [CrossRef]
27. Xu, C.; Gao, W. Pilling-Bedworth ratio for oxidation of alloys. *Mater. Res. Innov.* **2000**, *3*, 231–235. [CrossRef]
28. Li, T.F. *The High-Temperature Oxidation and Hot Corrosion of Metal*; Chemical Industry Press: Beijing, China, 2003.
29. Guo, Y.X.; Wang, H.L.; Liu, Q.B. Microstructure evolution and strengthening mechanism of laser-cladding $MoFe_xCrTiWAlNb$ refractory high-entropy alloy coatings. *J. Alloys Compd.* **2020**, *834*, 155147. [CrossRef]
30. Zheng, J.S.; Hou, X.M.; Wang, X.B.; Meng, Y.; Zheng, X.; Zheng, L. Isothermal oxidation mechanism of Nb-Ti-V-Al-Zr alloy at 700–1200 °C: Diffusion and interface reaction. *Corros. Sci.* **2015**, *96*, 186–195. [CrossRef]
31. Perepezko, J.; Bero, J.; Sakidja, R.; Talmy, I.; Zaykoski, J. Oxidation resistant coatings for refractory metal cermets. *Surf. Coat. Technol.* **2012**, *206*, 3816–3822. [CrossRef]
32. Li, H.; Wang, Y.; Fu, Q. Ablation resistance of carbides-coated C/C composites. *Surf. Eng.* **2017**, *33*, 803–809. [CrossRef]